Divergence of Voronoi Cell Anisotropy Vector: A Threshold-Free Characterization of Local Structure in Amorphous Materials

Jennifer M. Rieser,[*] Carl P. Goodrich,[†] Andrea J. Liu, and Douglas J. Durian

Department of Physics and Astronomy, University of Pennsylvania, Philadelphia, Pennsylvania 19104-6396, USA

Characterizing structural inhomogeneity is an essential step in understanding the mechanical response of amorphous materials. We introduce a threshold-free measure based on the field of vectors pointing from the center of each particle to the centroid of the Voronoi cell in which the particle resides. These vectors tend to point in toward regions of high free volume and away from regions of low free volume, reminiscent of sinks and sources in a vector field. We compute the local divergence of these vectors, where positive values correspond to overpacked regions and negative values identify underpacked regions within the material. Distributions of this divergence are nearly Gaussian with zero mean, allowing for structural characterization using only the moments of the distribution. We explore how the standard deviation and skewness vary with the packing fraction for simulations of bidisperse systems and find a kink in these moments that coincides with the jamming transition.

In glassy liquids and disordered solids, heterogeneities in local structure correlate with heterogeneous particle rearrangement dynamics arising from thermal fluctuations or applied mechanical load [1–6]. Characterizing local structural heterogeneity is therefore important in experiment—for example, via the network of contacts and force chains [7–10]—and as a step in understanding thermal and mechanical response. A simple and physically appealing measure of local structure that forms the basis of historically important theories of glassy dynamics and plasticity is free volume [11–14]. Regions that are underpacked have a larger local free volume, and, therefore, ought to rearrange or yield more easily. Though intuitive, free volume is inherently a concept based on hard spheres and only applies at densities below jamming.

Here we introduce a generalization of the concept of free volume that derives from the radical Voronoi network and, hence, applies in a consistent way to particles interacting via any interparticle potential at any density. Our measure, Q_k, is inspired by the observation that the center of a particle center deviates from the centroid of the corresponding Voronoi cell when the configuration is disordered. In two dimensions, it is defined as

$$Q_k \equiv (\nabla \cdot \mathbf{c})(A_k/\bar{A}), \tag{1}$$

where $\mathbf{c}$ is the interpolated field of vectors that point from particle centers to the corresponding Voronoi cell centroids, the divergence is taken over a Delaunay triangle k with area A_k, and $\bar{A}$ is the average of all A_k within the packing. By construction, Q_k is dimensionless and has zero mean. It is sensitive to local structural heterogeneity and—though purely geometrical—has a clear physical interpretation: positive (negative) values correspond to overpacked

(underpacked) regions. In addition to establishing a statistical correlation between Q_k and local relative free volume, we find that the distribution of Q_k values over a packing is nearly Gaussian, with mode and median nearly equal to the mean (zero); hence, it may be well described by just the standard deviation and the skewness.

As an illustration, we calculate Q_k for a system of soft disks at a series of packing fractions that are widely varied, from the dilute limit to well above the jamming transition. Morse and Corwin [15] have recently identified geometrical features, similarly based on Voronoi tessellations, that exhibit singularities at the jamming transition. Here we find the standard deviation and skewness of the Q_k distribution also exhibit kinks at the transition. Thus, there is a signature of the jamming transition in Q_k, a geometrical quantity with clear physical relevance.
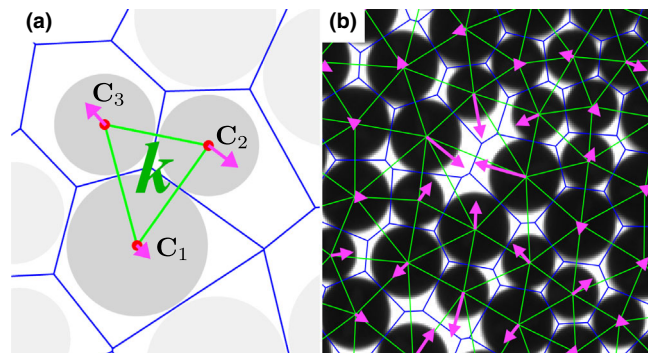

FIG. 1.   Particle packing from (a) simulation and (b) experiment [17,18], with superimposed radical Voronoi tesselation (blue) and Delaunay triangulation (green). Also shown are vectors $\mathbf{C}_p$ (magenta) that point from each particle center (red dot) to the centroid of its Voronoi cell. In (b), these are elongated by a factor of 8 for ease of visualization.

We begin by using the software package VORO++ [16] to determine the radical Voronoi tessellation, a space-filling generalization of the standard Voronoi construction to polydisperse systems. In this framework, each cell edge is determined from two adjacent circles, and is given by the locus of points from which tangent lines drawn to both circles have the same length. If all particle radii are equal, the standard Voronoi tessellation is recovered. Figure 1 shows an example where the Voronoi tessellation is overlaid on an image of particles. Any two particles with a shared Voronoi cell edge are defined as neighbors; from this, we generate a generalized Delaunay triangulation by connecting groups of three mutual neighbors into triangles, as shown in green in Fig. 1.

The position of a particle within its Voronoi cell is an indicator of local variation in the packing. This motivates consideration of a local anisotropy vector, $\mathbf{C}_p$, for each particle p, that points from the center of the particle to the centroid of its Voronoi cell, as shown by the magenta arrows in Fig. 1. In monodisperse crystalline packings with a single particle per unit cell, each particle center and the corresponding Voronoi cell centroid coincide; therefore, $\mathbf{C}_p = 0$ for all p, consistent with the idea that $\mathbf{C}_p$ is a measure of the structural anisotropy. This vector is one of several Minkowski functionals [19] associated with a Voronoi cell, many of which have been used to describe packing heterogeneity [20,21]. Additionally, $\mathbf{C}_p$ has been discussed in the context of structure in liquids [22,23], and has been found to be correlated with particle motion [22,24]. As might be expected, $\mathbf{C}_p$ points in the direction of excess free volume, indicating the direction in which the particle has the most space to move. However, local spatial variations of this vector have not been previously explored.

Figure 1(b) shows a typical example of $\mathbf{C}_p$ vectors for several particles in a bidisperse packing with particle size ratio of 3:4 and hard-sphere interactions. Vectors tend to point in toward locally less well-packed and away from locally more well-packed regions of the packing, reminiscent of sinks and sources in a vector field. Therefore, it is natural to consider the divergence of a field defined by interpolating the $\mathbf{C}_p$ vectors over a local region. We choose Delaunay triangles as the local regions over which to perform interpolation and differentiation of the $\mathbf{C}_p$ vectors. This allows us to use the framework of the constant strain triangle of finite element analysis [25] to find local spatial variations of the $\mathbf{C}_p$ vectors. In particular, each triangle is treated independently and we assume that the associated $\mathbf{C}_p$ vectors define a vector field $\mathbf{c} = (c_x, c_y)$ that varies linearly over each triangle,

$$c_x(x, y) = d_x + d_{xx}x + d_{xy}y,$$
$$c_y(x, y) = d_y + d_{yx}x + d_{yy}y. \qquad (2)$$

For each triangle the six constants $d_x, d_y, d_{xx}, d_{xy}, d_{yx}$, and d_{yy} can be determined by evaluating Eq. (2) at the triangle

vertices and inverting the resulting matrix equation. If the triangle coordinates are shifted so that the centroid of the triangle is located at the origin, the vector (d_x, d_y) is equivalent to $(\bar{c}_x, \bar{c}_y)$, where the averages are taken over the triangle vertices. The tensor $d_{ij} = \partial c_i / \partial x_j$ is independent of the origin location and describes the spatial variation of the $\mathbf{c}$ field over the triangle, with the divergence given by $\mathrm{Tr}(d_{ij})$.

From the divergence theorem, all contributions from interior particles cancel upon performing the sum $\sum_k Q_k$ over all triangles in a packing, leaving only contributions from the boundary particles. This results in $\langle Q_k \rangle = 0$ for infinite systems and for systems with periodic boundary conditions. The interpretation of Q_k is then physically intuitive: triangles with $Q_k < 0$ are less well packed than their surroundings, so we label these regions as underpacked, while triangles with $Q_k > 0$ are locally more tightly packed than their surroundings, so we refer to these regions as overpacked. Thus Q_k is a measure of relative free volume, and, as shown below, the statistical correlation is quantitative.

Figure 2(a) shows the probability density of Q_k for the experimental bidisperse system shown in Fig. 1(b). The probability density is nearly Gaussian with a small, positive mean resulting entirely from the finite boundaries of the packing. Thus, we may characterize packings to a great degree just from the standard deviation and skewness of the Q_k distribution. To the extent that the probability density is truly Gaussian and the Q_k values are spatially uncorrelated [26], the packing is random in a very simple sense. However, since adjacent triangles share two $\mathbf{C}_p$ vectors, there must be at least short-range correlations. Nevertheless, Q_k is closer to a Gaussian random variable than any other structural quantity previously used to characterize random packings. Furthermore, deviations from Gaussianity (e.g., underpacked particles in the tail of the distribution) are likely to have important physical consequences [27].

To build our intuitive understanding, we now compare Q_k with the local area fraction. Figure 2(b) shows the probability density for two standard measures, based on particle area per Voronoi cell and per Delaunay triangle. The probability densities for these quantities have irregular complicated shapes, where the median differs significantly from the mode for each distribution. There is no clear feature demarcating under- vs overpacked regions. Nevertheless, the magnitude of Q_k is on the order of—and statistically correlated with—the relative free area defined as $(\phi_k - \phi)/\phi$, where ϕ_k is the triangle-based area fraction and ϕ is the global area fraction of the sample. This is demonstrated by the contour plot of relative free area vs Q_k in the inset of Fig. 2(b). Similar plots in [26] show that good correlation holds at all packing fractions, but less so for dilute systems due to the development of long tails away from the heart of the distributions. We may thus consider
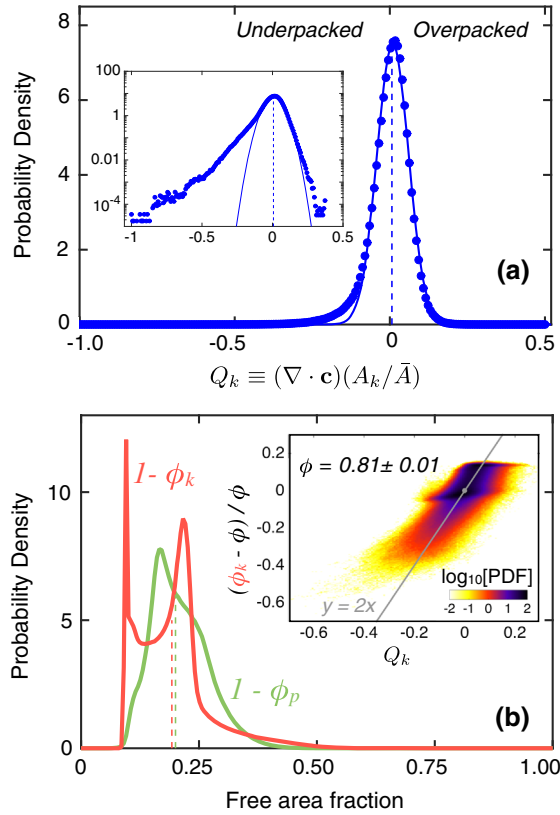
FIG. 2.   (a) Probability density of normalized divergence of center-to-centroid vectors for the experimental packing of bidisperse hard spheres shown in Fig. 1(b) (circles) and the best-fit Gaussian (solid curve). $Q_k > 0$ regions are more tightly packed than their surroundings; hence, we call these regions overpacked. $Q_k < 0$ regions are more loosely packed than their surroundings, and are therefore labeled underpacked. The inset shows the probability density and Gaussian fit with a logarithmic y axis, highlighting the deviation of the data from Gaussianity, particularly in the negative tail. (b) Probability density functions (PDFs) of triangle-based free area fraction, $1 - \phi_k$, and Voronoi-based free area fraction, $1 - \phi_p$, for the same packing. These distributions are more complicated and less intuitive than for Q_k. Inset: Q_k correlates well with a fractional deviation from the global packing fraction, and therefore is similar to a relative free area. All dashed lines indicate the median of the data set of the same color.

the size of Q_k as a semiquantitative indication of local free volume relative to the average packing.

For the remainder of the Letter, we use the Q_k distribution as a tool to characterize structure vs packing fraction for simulated systems in two dimensions. Static packings are created using four different protocols. For the first, a large number of points ($N = 5000$ to $N = 80000$) are placed at random in a box. For each N, we find that the average moments of Q_k over 200 configurations are independent of N. For the second protocol, we generate several packings of nonoverlapping monodisperse disks. Here, each disk has a radius equal to 1, and a proposed new disk is only accepted and placed in the box if it does not

overlap with any existing disks. These packings contain anywhere from $N = 1000$ to $N = 160000$ disks, spanning area fractions from $\phi \approx 0.003$ to $\phi \approx 0.5$. At least 40 packings are generated for each value of ϕ.

For the final two protocols, we numerically generate systems composed of $N = 2048$ soft repulsive disks with mass M. Two particles i and j interact with the pairwise potential

$$ V_{ij} = \frac{\epsilon}{2}\left(1 - \frac{r_{ij}}{R_i + R_j}\right)^2 \Theta\left(1 - \frac{r_{ij}}{R_i + R_j}\right), \quad (3) $$

where r_{ij} is the distance between the particle centers, R_i and R_j are the particle radii, $\Theta(x)$ is the Heaviside step function, and ϵ sets the energy scale. To prevent crystallization, we use a 50-50 mixture of particles with a size ratio of 1.4. The disks are initially placed at random in a periodic simulation box with a packing fraction ϕ, and are then allowed to move according to two different procedures. The units of length, mass, and energy are $2R_{\text{avg}}$, M, and ϵ, respectively, where $R_{\text{avg}} \equiv N^{-1}\sum_m R_m$ is the average particle radius.

For the third protocol, thermalized configurations are generated at a very low temperature using molecular dynamics simulations at constant NVT, performed using LAMMPS [28]. Beginning at a temperature of $T_{\text{start}} = 0.05$, we slowly cool the system to $T = 10^{-7}$ over 5×10^6 time steps. The system then remains at $T = 10^{-7}$ for an additional 10^7 time steps. The fourth and final protocol corresponds to an infinitely fast quench from infinite to zero temperature. Beginning with the initial random configuration, we minimize the total energy to a local minimum using the algorithm of Ref. [29]. Each protocol was repeated 500 times at each packing fraction.

For all final configurations, the Q_k distributions and moments are computed. The low-ϕ behavior of the standard deviation is emphasized in the main plot of Fig. 3(a). The results for protocols 2–4 appear to converge nicely to the value 0.5746 ± 0.0002 found from the random point patterns of protocol 1. Figure 3(b) shows a similar convergence of the skewness consistent with the value -2.086 ± 0.0002 obtained for point patterns. This validates the protocol methods, and serves to establish the low-ϕ "ideal gas" limiting behavior of the Q_k distributions.

As ϕ increases away from zero, the moments of the Q_k distribution change in a protocol-dependent fashion. As seen, the thermalized configurations are closer than the rapidly quenched configurations to the randomly placed nonoverlapping sphere configurations. The Q_k distributions all become narrower with increasing ϕ, as shown by the standard deviation plot. As judged from the skewness plot, the distributions generally become more Gaussian, as mentioned earlier. However, the quenched configurations show an initial increase in the skewness magnitude before decreasing towards zero.
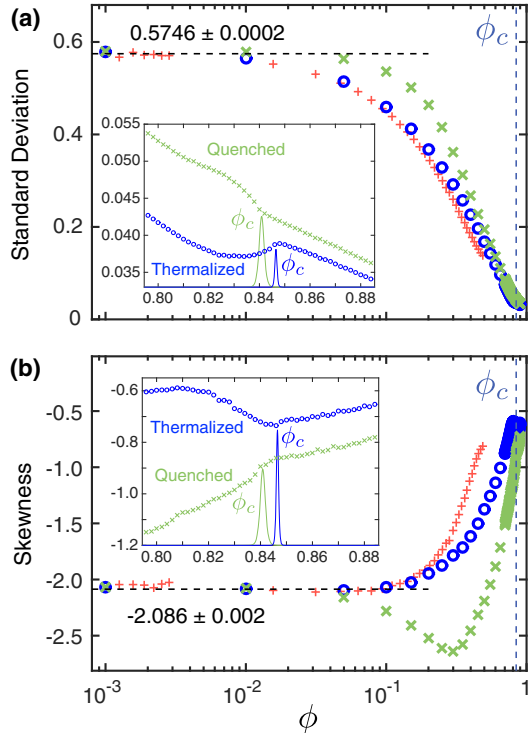
FIG. 3.   Standard deviation (a) and skewness (b) of the Q_k distributions vs global packing fraction ϕ. Each data point represents the average value of the specified moment over several configurations; the associated uncertainty is smaller than the symbol. The main plots emphasize the low-ϕ behavior, which approaches the same constant value for all preparation protocols shown: infinitely fast quench ($\times$), thermal ($\circ$), randomly placed nonoverlapping monodisperse circles ($+$), and random point patterns with $\phi = 0$ (dashed line). Insets show behavior near ϕ_c. Rescaled distributions of ϕ_c are plotted as solid curves, with the color indicating the preparation protocol from which they were determined. The moments of Q_k have a kink that coincides with the peak in the respective ϕ_c distribution.

The insets in Fig. 3 zoom in on the moments near the critical packing fraction ϕ_c, where the systems become jammed. For our simulations, there is a distribution of ϕ_c values due to the finite system size [30,31]. Each protocol produces a different distribution [32,33]. Here, the average and standard deviation are $\phi_c = 0.8409 \pm 0.0012$ for the quenched protocol and $\phi_c = 0.8465 \pm 0.0005$ for the thermalized protocol. As expected, the ϕ_c values are smaller and more widely distributed for quenched configurations, since thermalized configurations have more opportunity to relax [32]. The unnormalized ϕ_c distributions are individually rescaled to reach the respective data curves in the insets of Fig. 3, in order to mark the jamming transitions.

The striking key result evident in the Fig. 3 insets is that a signature of the jamming transition exists in the Q_k distributions. Namely, the standard deviation and the skewness both show a kink where the ϕ_c distributions are peaked. For the quenched protocol, the skewness kink is smaller and may deviate slightly from ϕ_c. For the

thermalized protocol, the behavior near ϕ_c is considerably more dramatic. In particular, the kinks are extremely pronounced in that the derivatives of standard deviation and of skewness vs ϕ actually change sign on opposite sides of the transition. Furthermore, there is nonmonotonic behavior below the transition, with the standard deviation and the skewness exhibiting a minimum and maximum, respectively, at a packing fraction a few percent below ϕ_c. As a measure of static structure vs ϕ, the Q_k distribution is thus even capable of signaling a precursor, i.e., that the onset of jamming is imminent. Because this happens for the thermalized but not the quenched configurations, it could be related to the dynamical hard-sphere glass transition; however, the extrema are at different ϕ values. Note that the differences in the trends for the two protocols implies that details of the local structure are sensitive to the protocol even though other quantities that are singular at the jamming transition, such as the average contact number, scale the same way with increasing pressure for packings prepared using different protocols [32].

In conclusion, we have shown that Q_k is a geometrical measure of structure, with the physical meaning of a relative free volume, that displays a strong signature of the jamming transition. It is particularly easy to interpret Q_k in terms of overpacked and underpacked regions since the Q_k distribution has zero mean, by construction, and is nearly Gaussian for nondilute systems. Though all our examples are two-dimensional, the concept of Q_k may be extended to any dimension by appropriate Voronoi construction. For thermal and sheared systems, there is longstanding interest in identifying structural features that lead to dynamical activity such as heterogeneous particle rearrangements and shear bands. The correlation of Q_k with dynamics, as well as with structural predictors of rearrangements found by machine learning [6], may now be studied. This could give new meaning to the concept of "free volume," which has been assumed to affect dynamics, and thereby to control the glass transition and glassy rheology, in many theories [13].

*jennifer.rieser@gatech.edu
Present address: School of Physics, Georgia Institute of Technology, Atlanta, Georgia 30332-0430, USA.
†Present address: School of Engineering and Applied Sciences, Harvard University, Cambridge, Massachusetts 02138, USA.

[1] C. P. Royall, S. R. Williams, T. Ohtsuka, and H. Tanaka, Nat. Mater. **7**, 556 (2008).

[2] M. Tsamados, A. Tanguy, C. Goldenberg, and J.-L. Barrat, Phys. Rev. E **80**, 026112 (2009).

[3] M. L. Manning and A. J. Liu, Phys. Rev. Lett. **107**, 108302 (2011).

[4] A. Malins, J. Eggers, C. P. Royall, S. R. Williams, and H. Tanaka, J. Chem. Phys. **138**, 12A535 (2013).

[5] R. L. Jack, A. J. Dunleavy, and C. P. Royall, Phys. Rev. Lett. **113**, 095703 (2014).

[6] E. D. Cubuk, S. S. Schoenholz, J. M. Rieser, B. D. Malone, J. Rottler, D. J. Durian, E. Kaxiras, and A. J. Liu, Phys. Rev. Lett. **114**, 108001 (2015).

[7] T. S. Majmudar and R. P. Behringer, Nature (London) **435**, 1079 (2005).

[8] K. W. Desmond, P. J. Young, D. Chen, and E. R. Weeks, Soft Matter **9**, 3424 (2013).

[9] I. Jorjadze, L.-L. Pontani, and J. Brujić, Phys. Rev. Lett. **110**, 048302 (2013).

[10] D. S. Bassett, E. T. Owens, M. A. Porter, M. L. Manning, and K. E. Daniels, Soft Matter **11**, 2731 (2015).

[11] D. Turnbull and M. H. Cohen, J. Chem. Phys. **34**, 120 (1961).

[12] F. Spaepen, Acta Metall. **25**, 407 (1977).

[13] G. Tarjus, in *Dynamical Heterogeneities in Glasses, Colloids, and Granular Media*, edited by L. Berthier, G. Biroli, J.-P. Bouchaud, L. Cipelletti, and W. van Saarloos (Oxford University Press, New York, 2011).

[14] M. Maiti and S. Sastry, J. Chem. Phys. **141**, 044510 (2014).

[15] P. K. Morse and E. I. Corwin, Phys. Rev. Lett. **112**, 115701 (2014).

[16] C. H. Rycroft, Chaos **19**, 041111 (2009).

[17] W. Li, J. M. Rieser, A. J. Liu, D. J. Durian, and J. Li, Phys. Rev. E **91**, 062212 (2015).

[18] J. M. Rieser, W. Li, J. Li, J. P. Gollub, and D. J. Durian (to be published).

[19] G. E. Schröder-Turk, S. Kapfer, B. Breidenbach, C. Beisbart, and K. Mecke, J. Microsc. **238**, 57 (2010).

[20] G. E. Schröder-Turk, W. Mickel, M. Schröter, G. W. Delaney, M. Saadatfar, T. J. Senden, K. Mecke, and T. Aste, Europhys. Lett. **90**, 34001 (2010).

[21] F. M. Schaller, S. C. Kapfer, J. E. Hilton, P. W. Cleary, K. Mecke, C. De Michele, T. Schilling, M. Saadatfar, M. Schröter, G. W. Delaney, and G. E. Schröder-Turk, Europhys. Lett. **111**, 24002 (2015).

[22] A. Rahman, J. Chem. Phys. **45**, 2585 (1966).

[23] J. Farago, A. Semenov, S. Frey, and J. Baschnagel, Eur. Phys. J. E **37**, 46 (2014).

[24] S. Slotterback, M. Toiya, L. Goff, J. F. Douglas, and W. Losert, Phys. Rev. Lett. **101**, 258001 (2008).

[25] R. D. Cook, *Concepts and Applications of Finite Element Analysis* (John Wiley and Sons, Inc., New York, 1974).

[26] See Supplemental Material at http://link.aps.org/supplemental/10.1103/PhysRevLett.116.088001 for semi-logarithmic plots of probability densities, correlations between relative free area and Q_k for numerous ϕ, non-area-weighted probability densities, spatial autocorrelations, and contact network sensitivities.

[27] T. H. Beuman, A. M. Turner, and V. Vitelli, Proc. Natl. Acad. Sci. U.S.A. **109**, 19943 (2012).

[28] S. Plimpton, J. Comput. Phys. **117**, 1 (1995).

[29] E. Bitzek, P. Koskinen, F. Gähler, M. Moseler, and P. Gumbsch, Phys. Rev. Lett. **97**, 170201 (2006).

[30] C. S. O'Hern, S. A. Langer, A. J. Liu, and S. R. Nagel, Phys. Rev. Lett. **88**, 075507 (2002).

[31] C. S. O'Hern, L. E. Silbert, A. J. Liu, and S. R. Nagel, Phys. Rev. E **68**, 011306 (2003).

[32] P. Chaudhuri, L. Berthier, and S. Sastry, Phys. Rev. Lett. **104**, 165701 (2010).

[33] D. Vågberg, P. Olsson, and S. Teitel, Phys. Rev. E **83**, 031307 (2011).